The incorporation of an organic soil layer in the Noah-MP Land Surface Model and its evaluation over a Boreal Aspen Forest

Liang Chen[1, 2], Yanping Li[1], Fei Chen[3], Alan Barr[4], Michael Barlage[3], and Bingcheng Wan[3]

[1]Global Institute for Water Security, University of Saskatchewan, Saskatoon, SK, Canada

[2]Key Laboratory of Regional Climate Environment for Temperate East Asia, Institute of Atmospheric Physics, Chinese Academy of Sciences, Beijing, China

[3]National Center for Atmospheric Research, Boulder, Colorado

[4]Environment Canada, National Hydrology Research Center, Saskatoon, SK, Canada

Corresponding author address:

Yanping Li

Global Institute for Water Security

School of Environment and Sustainability

University of Saskatchewan

Phone: 306-966-2793

E-mail: yanping.li@usask.ca

Abstract

A thick top layer of organic matter is a dominant feature in boreal forests and can impact land-atmosphere interactions. In this study, the multi-parameterization version of the Noah land-surface model (Noah-MP) was used to investigate the impact of incorporating a forest-floor organic soil layer on the simulated surface energy and water cycle components at the BERMS Old Aspen Flux (OAS) field station in central Saskatchewan, Canada. Compared to a simulation without an organic soil parameterization (CTL), the Noah-MP simulation with an organic soil (OGN) improved Noah-MP simulated soil temperature profiles and soil moisture at 40-100cm, especially the phase and amplitude (Seasonal cycle) of soil temperature below 10 cm. OGN also enhanced the simulation of sensible and latent heat fluxes in spring, especially in wet years, which is mostly related to the timing of spring soil thaw and warming. Simulated top-layer soil moisture is better in OGN than that in CTL. The effects of including an organic soil layer on soil temperature are not uniform throughout the soil depth and are more prominent in summer. For drought years, the OGN simulation substantially modified the partitioning of water between direct soil evaporation and vegetation transpiration. For wet years, the OGN simulated latent heat fluxes are similar to CTL except for spring season where OGN produced less evaporation, which was closer to observations. Including organic soil produced more sub-surface runoff and resulted in much higher runoff throughout the freezing periods in wet years.

Keywords Organic soil, Noah-MP, surface energy and water budgets, BERMS

1. Introduction

Land surface processes play an important role in the climate system by controlling land-atmosphere exchanges of momentum, energy and mass (water, carbon dioxide, and aerosols). Therefore, it is critical to correctly represent these processes in land surface models (LSMs) that are used in weather prediction and climate models (e.g., Dickinson et al. 1986; Sellers et al. 1996; Chen and Dudhia 2001; Dai et al. 2003; Oleson et al. 2008, Niu et al. 2011). Niu et al. (2011) and Yang et al. (2011) developed the Noah LSM with multi-parameterization options (Noah-MP) and evaluated its simulated seasonal and annual cycles of snow, hydrology, and vegetation in different regions. Noah-MP has been implemented in the community Weather Research and Forecasting (WRF) model (Barlage et al. 2015), which is widely used as a numerical weather prediction and regional climate model for dynamical dowscaling in many regions world-wide (Chotamonsak et al., 2012). The performance of Noah-MP was previously evaluated using in-situ and satellite data (Niu et al. 2011, Yang et al. 2011, Cai et al. 2014, Pilotto et al. 2015, Chen et al. 2014). Those evaluation results showed significant improvements in modeling runoff, snow, surface heat fluxes, soil moisture, and land skin temperature compared to the Noah LSM (Chen et al. 1996, Ek et al. 2003). Recently, Chen et al. (2014) compared Noah-MP to Noah and four other LSMs regarding the simulation of snow and surface heat fluxes at a forested site in the Colorado Headwaters region, and found a generally good performance of Noah-MP. However, it is challenging to parameterize the cascading effects of snow albedo and below-canopy turbulence and radiation transfer in forested regions as pointed out by Clark et al. (2015) and Zheng et al. (2015).

The Canadian boreal region contains one third of the world's boreal forest, approximately 6 million km^2 (Bryant et al. 1997). The boreal forests have complex interactions with the

atmosphere and have significant impacts on regional and global climate (Bonan, 1991; Bonan et al., 1992; Thomas and Rowntree, 1992; Viterbo and Betts, 1999; Ciais et al., 1995). Several field experiments were conducted to better understand and model these interactions, including BOREAS (Boreal Ecosystem Atmosphere Study) and BERMS (Boreal Ecosystem Research and Monitoring Sites). Numerous studies have evaluated LSMs using the BOREAS and BERMS data (Bonan et al. 1997). Levine and Knox (1997) developed a frozen soil temperature (FroST) model to simulate soil moisture and heat flux and used BOREAS northern and southern study areas to calibrate the model. They found that soil temperature was underestimated and large model biases existed when snow was present. Bonan et al. (1997) examined NCAR LSM1 with flux-tower measurements from the BOREAS, and found that the model reasonably simulated the diurnal cycle of the fluxes. Bartlett et al. (2002) used the BOREAS Old Jack Pine (OJP) site to assess two different versions of CLASS, the Canadian Land Scheme (2.7 and 3.0) and found that both versions underestimated the snow depth and soil temperature values, especially the version CLASS 2.7.

Boreal forest soils often have a relatively thick upper organic horizon. The thickness of the organic horizon directly affects the soil thermal regime and soil hydrological processes. Compared with mineral soil, the thermal and hydraulic properties of the organic soil are significantly different. Dingman (1994) found that the mineral soil porosity ranges from 0.4 to 0.6, while the porosity of organic soil is seldom less than 0.8 (Radforth et al., 1977). The hydraulic conductivity of organic soil horizons can be very high due to the high porosity (Boelter, 1968). Less suction is observed for given volumetric water content in organic soils than in mineral soils except when it reaches saturation. The thermal properties of the soil are also affected by the underground hydrology. Organic soil horizons also have relatively low thermal

47 conductivity, relatively high heat capacity and a relatively high fraction of plant-available water.
48 Prior studies illustrated the importance of parameterizing organic soil horizons in LSMs for
49 simulating soil temperature and moisture (e.g., Letts et al. 2000, Beringer et al. 2001, Molders
50 and Romanovsky 2006, Nicolsky et al. 2007, Lawrence and Slater 2008).

51 The current Noah-MP model does not include a parameterization for organic soil
52 horizons. It is thus critical to evaluate the effects of incorporating organic matter on surface
53 energy and water budgets in order to enhance the global applicability of the WRF-Noah-MP
54 coupled modeling system. Here we conduct a detailed examination of the performance of the
55 Noah-MP model in a Canadian boreal forest site. The main objective of this research is to
56 enhance the modeling of vertical heterogeneity (such as organic matter) in soil structures and to
57 understand its impacts on the simulated seasonal and annual cycle of soil moisture and surface
58 heat fluxes. We recognize that Noah-MP has weaknesses in existing sub-process
59 parameterizations, while the goal of this study is to explore the impact of incorporating organic
60 soil on surface energy and water budgets, rather than comprehensively addressing errors in
61 existing Noah-MP parameterization schemes. In this paper, we present the BERMS observation
62 site in central Saskatchewan (Section 2), and our methodology for conducting 12-year Noah-MP
63 simulations with and without organic soil layer for that boreal forest site (Section 3). Section 4
64 discusses the simulations of the diurnal and annual cycles of the surface energy and hydrological
65 components, in dry and wet periods. Summary and conclusions are given in Section 5.
66

67 **2. BERMS site descriptions**

68 The Old Aspen Site (OAS, 53.7°N, 106.2°W, altitude 601 m) is located in mature
69 deciduous broadleaf forest at the southern edge of the Canadian boreal forest in Prince Albert

National Park, Saskatchewan, Canada (Figure 1). The forest canopy consists of a 22-m trembling aspen overstory (*Populus tremuloides*) with ~10% balsam poplar (*Populus balsamifera*.) and a 2-m hazelnut understory (*Corylus cornuta*) with sparse alder (*Alnus crispa*). The fully-leafed values of the leaf area index varied among years from 2.0 to 2.9 for the aspen overstory and 1.5 to 2.8 for the hazelnut understory (Barr et al. 2004). The forest was regenerated after a natural fire in 1919, and in 1998 it had a stand density of ~830 stems ha^{-1}. The soil is an Orthic Gray Luvisol (Canadian Soil Classification System) with an 8-10 cm deep forest-floor (LFH) organic horizon overlying a loam Ae horizon (0-21 cm), a sandy clay loam Bt horizon (21-69 cm), and a sandy clay loam Ck horizon (69+ cm). 30% of the fine roots are in the LFH horizon and 60% are in the upper 20 cm of mineral soil. The water table lies from 1 to 5 m below the ground surface, varying spatially in the hummocky terrain and varying in time in response to variations in precipitation. A small depression near the tower had ponded water at the surface during the wet period from 2005 to 2010. Mean annual air temperature and precipitation at the nearest long-term weather station are 0.4 °C and 467 mm, respectively (Waskesiu Lake, 53°55'N, 106°04'W, altitude 532 m, 1971-2000 climatic normal).

Air temperature and humidity were measured at 36-m above ground level using a Vaisala model HMP35cf or HMP45cf temperature/humidity sensor (Vaisala Oyj, Helsinki, Finland) in a 12-plate Gill radiation shield (R.M. Young model 41002-2, Traverse City, MI, USA). Windspeed was measured using a propeller anemometer (R.M. Young model 01503-, Traverse City, MI, USA) located at 38-m above ground level. Atmospheric pressure was measured using a barometer (Setra model SBP270, distributed by Campbell Scientific Inc., Logan, UT, USA). Soil temperature was measured using thermocouples in two profiles at depths of 2, 5, 10, 20, 50 and 100 cm. The two upper measurements were in the forest-floor LFH. Soil volumetric water

content was measured using TDR probes (Moisture Point Type B, Gabel Corp., Victoria, Canada) with measurements at depths of 0-15, 15-30, 30-60, 60-90 and 90-120 cm. Three of the eight probes that were the most free of data gaps were used in this analysis. The TDR probes were located in a low-lying area of the site that was partially flooded after 2004, resulting in high Volumetric Water Content (VWC) values that may not be characteristic of the flux footprint. VWC is also measured at 2.5- and 7.5-cm depth in the forest-floor LFH layer using two profiles of soil moisture reflect meters (model CS615, Campbell Scientific Inc., Logan, UT, USA), inserted horizontally at a location that did not flood.

Eddy-covariance measurements of the sensible and latent heat flux densities were made at 39 m above the ground from a twin scaffold tower. Details of the eddy-covariance systems are given in Barr et al. (2006). Data gaps were filled using a standard procedure (Amiro et al. 2006).

The net radiation flux density, Rn, was calculated from component measurements of incoming and outgoing shortwave and longwave radiation, made using paired Kipp and Zonen (Delft, The Netherlands) model CM11 pyranometers and paired Eppley Laboratory (Newport, RI, USA) model PIR pyrgeometers. The upward-facing radiometers were mounted atop the scaffold flux tower in ventilated housings to minimize dew and frost on the sensor domes. The net radiometer and the downward-facing radiometers were mounted on a horizontal boom that extended 4 m to the south of the flux tower, ~ 10 m above the forest canopy. Details of the minor terms in the surface energy balance; including soil heat flux and biomass heat storage flux are given in Barr et al. (2006). During the warm season when all components of the surface energy balance were resolved, the sum of the eddy-covariance sensible and latent heat fluxes underestimated the surface available energy (net radiation minus surface storage) by ~15% (Barr et al. 2006).

3. Methodology

3.1 The Noah-MP Land-Surface Model

Noah-MP is a new-generation of LSM, which was developed to improve the performance of the Noah LSM (Chen et al. 1996; Chen and Dudhia 2001). It is coupled to the WRF community weather and regional climate model (Barlage et al. 2015), and also available as a stand-alone 1-D model (Noah-MP v1.1). Noah-MP simulates several biophysical and hydrological processes that control fluxes between the surface and the atmosphere. These processes include surface energy exchange, radiation interactions with the vegetation canopy and the soil, hydrological processes within the canopy and the soil, a multi-layer snowpack with freeze-thaw, groundwater dynamics, stomatal conductance, and photosynthesis and ecosystem respiration. The major components include a 1-layer canopy, 3-layer snow, and 4-layer soil. Noah-MP provides a multi-parameterization framework that allows using the model with different combinations of alternative process schemes for individual processes (Niu et al., 2011). Alternative sub-modules for 12 physical processes can provide more than 5000 different combinations. Soil water fluxes are calculated by the Richards equation using a Campbell/Clapp-Hornberger parameterization of the hydraulic functions (Clapp and Hornberger, 1978).

We use an off-line stand-alone 1-D mode (Noah-MP) with four soil layers: 0-10cm, 10-40cm, 40-100cm, and 100-200 cm. The selected Noah-MP physics options used in this study are similar to Barlage et al. (2015), Gao et al. (2015) and Chen et al. (2014) and are list in Table 1. In the default configuration of Noah-MP, the entire vertical soil profile was treated as one mineral ground texture only, and no organic soil matter is included.

The OAS research site has an organic LFH (forest-floor) soil horizon, 8~10 cm deep. This study evaluates the impact of adding an organic soil horizon in the Noah-MP model using a similar approach to Lawrence and Slater (2008), which parameterizes soil thermal and hydrologic properties in terms of carbon density in each soil layer. Soil carbon or organic fraction for each layer is determined as

$$f_{sc,i} = \frac{\rho_{sc,i}}{\rho_{sc,\max}} \quad (1)$$

where $f_{sc,i}$ is the carbon fraction of the each layer, $\rho_{sc,i}$ is the soil carbon density, and $\rho_{sc,\max}$ is the maximum possible value (peat density of 130 kg m^{-3}, Farouki 1981). In this study, we assume that the top-soil layer is made up of 100% organic matter, consistent with the 8-10 cm LFH horizon at OAS, with the carbon fraction equals to 1. The soil properties for this layer are calculated based on the parameters of organic soil. The second layer of the soil is considered as transition layer and made up of 30% organic matter with the carbon fraction equals to 0.3. The soil properties for this layer are specified as a weighted combination of organic and mineral soil properties:

$$\boldsymbol{P = \left(1 - f_{sc,i}\right)P_m + f_{sc,i}P_o} \quad (2)$$

where P_m is the value for mineral soil, P_o is the value for organic soil, and P is the weighted average. The remaining soil layers were assumed to be 100% mineral soil, with the carbon fraction equals to 0, the soil properties for this layer are calculated based on the parameters of mineral soil. To investigate impacts of uncertainties of those parameters on simulations, we conducted sensitive tests for key parameters such as saturated hydraulic conductivity, porosity, suction, and Clapp and Hornberger parameter. Those parameters were perturbed within a 5-20% range (except for hydraulic conductivity that is changed over 4 times below and above the

default value) following the work of Letts et al. (2000). Results showed that the simulated top layer soil moisture is very sensitive to porosity, saturate hydraulic conductivity, saturated matric potential and Clapp and Hornberger parameter, while other layers are not too sensitive to those parameters. For porosity, as the value increased, the top soil moisture increased significantly. The saturated hydraulic conductivity mainly influences the unfrozen period. As the value increased, the top soil moisture decreased. Saturated matric potential and the Clapp and Hornberger parameter only influence the frozen period. For saturated matric potential, the top soil moisture decreased when the parameter value increased. While for Clapp and Hornberger parameter, the top soil moisture increased when the parameter value increased. Based on the site measurement, the soil bulk density of the top layer is about 160 kg m^{-3}. As described in Letts et al. (2000), this organic soil can be defined as hemic peat, a medium humified organic soil. Table 2 gives the recommended parameters for hemic peat, with 0.88, 2.0, 0.0102, and 6.1 for porosity, saturated hydraulic conductivity, saturated matric potential and Clapp and Hornberger parameter, respectively (Letts et al., 2000). From the sensitivity test mentioned above, it seems that the recommended values from Letts et al. (2000) produced soil moisture and soil temperature close to observations.

3.2 Forcing data

The 30-min meteorological observations, including air temperature, specific humidity, wind speed, pressure, precipitation, downward solar, and longwave radiation, at 36-m height from OAS were used as atmospheric forcing data to drive Noah-MP in an off-line 1-D mode. Figure 2 shows the annual mean temperature (1.5 ^{o}C) and total precipitation (406 mm) at this site during the study period (1998-2009). The most significant climatic features during the study

183 period are a prolonged drought that began in July 2001 and extended throughout 2003, and an
184 extended wet period from 2004-2007.
185
186 *3.3 Evaluation of model performance*
187 Outputs from the Noah-MP simulations were evaluated against observations, using the
188 Root Mean Squared Error (RMSE), square of the correlation coefficient (R^2), and Index of
189 Agreement (IOA) (Zhang et al. 2013). The IOA is calculated as

190 $$IOA = 1 - \frac{\sum_{i=1}^{N}(M_i - O_i)^2}{\sum_{i=1}^{N}(|O_i - \overline{O}| + |M_i - \overline{O}|)^2} \quad (3)$$

191 Where M_i and O_i are simulated and observed values of the same variable, respectively, and $\overline{O}$
192 is the mean of the observed values. IOA ranges from 0 (no agreement) to 1 (perfect match).
193
194 **4. Results and Discussions**
195 *4.1 Noah-MP model Spin-up*
196 The LSM spin-up is broadly defined as an adjustment processes as the model approaches
197 its equilibrium following the initial anomalies in soil moisture content or after some abnormal
198 environmental forcing (Yang et al., 1995). Without spin-up, the model results may exhibit drift
199 as model states try to approach their equilibrium values. To initialize LSMs properly, the spin-up
200 time required for LSMs to reach the equilibrium stage needs to be examined first (Chen and
201 Mitchell 1999, Cosgrove et al. 2003). In this study, model runs for the year 1998 were performed
202 repeatedly until all the soil-state variables reached the equilibrium state, defined as when the
203 difference between two consecutive one-year simulations becomes less than 0.1% for the annual

means (Cai et al., 2014; Yang et al., 1995). Yang et al. (1995) discussed the spin-up processes by comparing results from 22 LSMs for grass and forest sites, and showed a wide range of spin-up timescales (from 1 year to 20 years), depending on the model, state variable and vegetation type. Cosgrove et al. (2003) used four NLDAS-1 LSMs to discuss the spin-up time at six sub-regions covering North America, and showed that all models reached equilibrium between one to three years for all six sub-regions. In this study, we found that it requires 9 years for deep-soil moisture (100-200 cm layer) in Noah-MP to reach its equilibrium, 8 years for latent heat flux and evapotranspiration, but only 3 years for the surface soil moisture (Figure 3). Cosgrove et al. (2003) and Chen et al. (1999) indicated that it takes long time to reach equilibrium especially in the deep soil layers and sparse vegetation because the evaporation was limited by slow water diffusion time scales between the surface and deep soil layers. When using the groundwater component of Noah-MP, it might take at least 250 years to spin-up the water table depth in arid regions (Niu et al., 2007). Cai et al. (2014) found that water table depth requires less than 10 years to spin-up in a wet region, but more than 72 years for a dry region. For this boreal forest site where the water table depth is shallower (less than 2.5 m), it takes ~7 years for water table depth to reach equilibrium. However, the freezing/thawing is a relatively slow process, so we set 10 years for the spin-up time for all the experiments discussed here.

4.2 Seasonal cycle of soil temperature and moisture

We defined the simulation without incorporating organic soil as the "control experiment" (CTL); the simulation with the organic soil incorporated as the "organic layer experiment" (OGN). We first evaluated the CTL and OGN simulated soil temperature and moisture at the OAS site in relation to observations for the period of 1998-2009.

As shown in Figure 4, the effects of including a 10-cm organic top soil layer on simulated soil temperature are not uniform both throughout the soil depth and during the year. Figure 4a shows the CTL and OGN simulations produced nearly identical top-layer temperature which are in agreement with the observations except for a low bias in the winter period, especially during drought years 2002-2003. However, for deep layers (10-100cm), soil temperature from the OGN is lower (higher) than the CTL simulation during summer (winter), especially for the drought years 2002-2003, leading to a good agreement between OGN and observations for 2^{nd} and 3^{rd} layer soil temperature (Figure 4b, c). Lawrence and Slater (2008) indicated that strong cooling in summer is due to the modulation of early and mid-summer soil heat flux, while higher soil temperature in fall and winter is due to less efficient cooling of organic soils. The soil thawing period in spring is significantly affected by the OGN parameterization since the thermal conductivity of the organic horizon is much lower than that of the mineral soil (~0.4 W m^{-1} K^{-1} compared to ~2.0 W m^{-1} K^{-1}), which delays the warming of the deep soil layers after snowmelt. In winter, the organic soil layer insulates the soil and results in relatively higher wintertime soil temperatures for OGN compared with CTL. The difference is most pronounced in drought years (2002 and 2003) (Figure 4). In summer, dues to lower saturated thermal conductivity (0.25 W/m K for organic compared to ~6.04 W/m K for mineral) in OGN, the downward transfer of hear from topsoil layer is less and the deep soil temperature in OGN is lower than that in CTL.

In winter, with the presence of soil ice, the thermal heat conductivity in OGN (~2.20 W/m K) is lower than that in CTL (6.04 W/m K), it reduces the upward transfer of heat from deep soils to topsoil and therefore results in higher deep-soil temperature in OGN. These results are consistent with studies that showed a simulated increase in winter soil temperature of up to 5 ^{o}C in boreal regions when including an organic layer (Koven et al., 2009; Rinke et al., 2008; Lawrence and Slater, 2008) in LSMs.

For the top soil layer, the OGN parameterization increases the liquid soil water content in summer as water fills the larger pore space of organic soil, though the liquid soil water content in winter didn't change much, due to the contrasting water retention characteristics of organic and mineral soil (Koven et al., 2009; Rinke et al., 2008; Lawrence and Slater, 2008). Higher porosity in OGN leads to an increase in total soil water content, while lower the topsoil temperature (Figure 4a) in OGN enhances the ice content. Note that the observed soil water content during wet years may be higher than the site truth because the sensors were located in a low spot that is prone to flooding. This site got flooded in 2004 and the ground water has not dried since then, so that the soil was oversaturated during the period of 2004-2008. In the second soil layer, the observed soil water content was incorrect after the site got flooded (2004-2008). With more precipitation during the wet period, the real soil water content should have a relatively high value. Since the OGN increases the soil water content, it should be closer to the true observation. From Figure 5, it can be seen that the OGN improved the liquid water simulation in non-frozen periods. The soil moisture data are not reliable when the soil is frozen and are therefore not very useful during the winter. In late spring when snow starts melting, both CTL and OGN simulate the same topsoil temperature (Figure 4). It is clear that the soil liquid water content is mainly controlled by precipitation, soil hydraulic conductivity and runoff. The high porosity of organic soil in the topsoil layer helps to retain more snowmelt water and hence increases the topsoil layer liquid water content. For the deep soil layers, the soil liquid water content is highly influenced by the soil temperature. Liquid soil water content increases during soil ice thawing period. The higher deep soil layer liquid water content in OGN is mainly because the soil hydraulic conductivity is higher for organic soil than mineral soil, so liquid water in the first-layer can be transported downward quickly into the deeper layers. Although the organic soil layer is only

added to the first two layers in this study, it still can affect the deep layer due to the infiltration characteristics of the topsoil.

The water retention characteristics of the organic soil horizon favor both higher water retention and reduced evaporation. The thermal conductivity is lower compared with that of the mineral soil, which then prevents the deeper soil to warm up rapidly after snowmelt season. The lower thermal conductivity of the top organic soil affects the annual cycle of the ground heat flux. In summer, the top layer is warmer than the deep layers, the ground heat flux then transfers heat downward. Because air temperature is lower than land surface temperature so heat is transferred upward from soil to the land surface, the low thermal conductivity of the organic soil can prevent the soil to cool. On the other hand, the snowfall in winter may form a snow layer that will insulate the soil and make the simulations less sensitive to thermal conductivity. This may be the reason why the OGN simulated winter soil temperature is higher compared to CTL simulations. With the organic soil layer on the top, the reduction of surface layer saturation levels in winter time (Figure 5) reduces the heat loss through evaporation. The winter soil temperature then becomes significantly higher compared with CTL experiment. On the contrary, the higher soil water content in the topsoil layer during summer time (Figure 5) increases the heat loss through evaporation, the summer soil temperature then becomes significantly lower compared with CTL experiment.

4.3 Seasonal cycles of sensible and latent heat flux

Simulated differences in top-layer soil temperature and liquid soil water content lead to the differences in simulated surface energy fluxes. Figure 6 show that the CTL run captures the observed monthly mean daytime sensible heat and latent heat flux reasonably well. However, SH

297 is underestimated in spring and overestimated in summer. Accordingly, LH is overestimated in
298 spring and underestimated in summer during most of the time period except for drought years
299 2002-2003 where LH is slightly overestimated. Generally, the OGN simulations show similar
300 characteristics to the CTL, with improved correlation coefficients between observations and
301 simulations: increasing from 0.88 (CTL) to 0.92 (OGN) for SH and from 0.94 (CTL) to 0.96
302 (OGN) for LH (Figure 7). Overall, both CTL and OGN perform well in winter when snow is
303 present and fluxes are small. During the spring snow-melting season, the OGN results are much
304 better than the CTL (Figures 6 and 7).

305 The OGN simulations also improved the underestimation of SH in spring in CTL, but it
306 still overestimates summer SH. The reason for high bias in summer SH will be further discussed
307 in Section 4.4. SH and especially LH show improvement in OGN compared to CTL, which is
308 related to timing of soil thaw and warming in spring. CTL thaws the soil too early causing a
309 premature rise in LH in spring (April-May) and an associated underestimation of spring SH. The
310 spring (April-May) fluxes are much improved in the OGN parameterization. However, both
311 OGN and CTL retain a serious positive bias in SH from June-September, especially for wet years.
312 The reduction of surface layer saturation levels in OGN led to lower soil evaporation and
313 associated reductions in the total latent heat flux, and the reduction of LH is accompanied by a
314 rise in SH (Figure 6).

315

316 *4.4 Impact of organic soil on diurnal cycle of surface energy and hydrology*

317 The quality of nighttime flux-tower data is questionable (Chen et al. 2015), especially for
318 OAS located in a boreal forest. Therefore, we focused our analysis on daytime observation data.
319 In general, the OGN parameterization improved the simulation of daily daytime LH in terms of

320 both RMSE and IOA, and increased IOA for SH (Table 3). Nevertheless, compared with CTL,
321 OGN increased the bias in SH slightly by ~3% (Table 3).

322 For the 12-year simulation period, the study site experienced a prolonged drought,
323 beginning in July 2001 and extended throughout 2002 and 2003. We choose year 2002 and 2003
324 to represent typical drought years, and year 2005 and 2006 to represent typical wet years (Figure
325 2), to examine the effect of the organic soil under different climate conditions. For drought years
326 2002-2003, OGN increased daytime SH especially in spring, and slightly decreased SH at
327 nighttime (Figure 8a, b, c, and d). LH is well simulated in both OGN and CTL (Figure 8e, f, g,
328 and h), with slightly increased daytime LH in OGN. OGN overestimates daytime SH compared
329 with observations, while CTL underestimates daytime SH for spring (Figure 8a). Both OGN and
330 CTL overestimates SH for summer, autumn and winter (Figure 8b, c, d).

331 For wet years (Figure 9), OGN produces in general higher daytime SH than CTL. For
332 spring, OGN simulated SH agrees with the observation better than CTL, but it is similar to or
333 slightly worse than CTL for other seasons. Simulated LH for both OGN and CTL agree with
334 observations well, with an improvement by OGN in spring, because the snowmelt process
335 dominates during spring months. For other seasons, the OGN results are close to CTL.

336 It is clear from Figures. 4, 8 and 9 that in both CTL and OGN, summer sensible heat
337 fluxes are overestimated for wet and dry years. We hypothesized that such high bias in summer
338 sensible heat flux is partly attributed to energy imbalance in observations. We then calculated the
339 energy balance residual term: Rnet-(SH+LH+G) for summer month (June, July, and August). In
340 wet years, G in CTL and OGN is close to observed values; modeled latent heat flux is
341 underestimated by ~10 W/m^2; modeled sensible heat flux is overestimated by ~30 W/m^2; and the
342 residual term is ~17 W/m^2. Hence, it is reasonable to argue that the surface energy imbalance

343 (~17 W/m^2) in observations contributes to a large portion of the ~30 W/m^2 high bias in sensible
344 heat fluxes. In dry years, the summer energy imbalance (~15 W/m^2) is nearly equal to the high
345 bias in sensible heat flux (~15 W/m^2).
346
347 *4.5 Impact of an organic soil horizon on annual cycle of surface energy and hydrology*
348 In the previous section, it is clear that the incorporation of the top organic layer helps
349 improve the simulation of the diurnal cycle of the surface energy and hydrologic components in
350 spring season. In the following, we focus on a detailed analysis of the annual cycle of the surface
351 energy and hydrology variables for "dry" (Figure 10) versus "wet" years (Figure 11). Between
352 June and September as shown in Figure10h, the upper two soil layers were unfrozen. The topsoil
353 is wetter in OGN for both dry and wet years compared with CTL because organic soil can retain
354 more water. As discussed in section 4.2, for the deep soil layers, the liquid water content is
355 influenced by the soil temperature and the movements of the soil liquid water content between
356 soil layers. Since the soil hydraulic conductivity is higher for OGN than mineral soil, the water
357 moves faster into deep soil layers than CTL, therefore the OGN simulates higher soil liquid
358 water content in deep layers. OGN has a major impact on the daily cycle of soil temperature.
359 Consistent with discussions in Section 4.2, the soil temperature below 10 cm simulated by OGN
360 is lower in summer and higher in winter than that of the CTL simulation, and the OGN
361 simulation shows less bias than the CTL simulation (Figure 4). In OGN simulation, the water
362 moves faster into deep layers than in CTL simulation, leading to more infiltrated water in the
363 deep soil and hence higher base flow. Consequently, the total runoff is increased. Due to the high
364 soil porosity of the organic soil, OGN simulation shows higher soil-ice fraction at the top soil
365 layer during the freezing periods. The higher water capacity and higher soil-ice fraction of the

366 organic soil then reduce liquid water content/soil moisture, leading to less evaporation (i.e.,
367 latent heat flux) during spring freezing periods, and a compensating increase of the sensible heat
368 flux.

369 By adding an organic soil layer, the soil ice content becomes higher due to higher
370 porosity. For dry years, the impact of the organic soil on surface and sub-surface runoff is not
371 significant (Figure 10e, f). The increase in the summer latent heat flux and sensible heat flux are
372 compensated by a decrease in soil heat flux, leading to a significant decrease in summer soil
373 temperature. In winter, the latent and sensible heat fluxes are not modified by the organic soil,
374 but increased soil heat flux leads to an increased soil temperature in winter. The most prominent
375 change by adding organic soil layer is the partition between vegetation transpiration and direct
376 ground evaporation (Figure 12a and b) where the OGN simulation slightly increased ground
377 surface evaporation and vegetation transpiration.

378 For wet years (Figure 11), the impact of the organic soil on surface and sub-surface
379 runoff becomes more significant, especially for sub-surface runoff. The organic soil decreases
380 the surface runoff during the summer season, and increases the sub-surface runoff during the
381 freezing periods while decreases the sub-surface runoff during summer season. Because of the
382 higher surface layer soil ice content, the increase of subsurface flow should be due to the
383 producing a wetter soil profile by OGN. The sensible heat flux also increases significantly in
384 spring, with an associated reduction in latent heat flux and soil heat flux. The summer soil
385 temperature also decreases but to a lesser degree than that in dry years, because the soil heat flux
386 decreases less compared with dry years. Unlike dry years, there is a significant runoff change in
387 wet years, and the ground evaporation is also decreased (Figure 12c and d). OGN produces more
388 soil-ice content and higher soil porosity, and leads to higher soil water content than CTL

389 simulations as the higher ice content severely restricts movement of water out of the soil column.
390 In wet season, by adding an organic topsoil layer, the soil water increases due to the infiltration
391 of the soil water into the deep soil. This then leads to an increase in the sub-surface runoff. As a
392 consequence, the volumetric liquid water becomes higher in summer for OGN compared with
393 CTL simulation.
394
395 **5. Summary and Conclusions**
396 In this study, the Noah-MP LSM was applied at the BERMS Old Aspen site to
397 investigate the impact of incorporating a realistic organic soil horizon on simulated surface
398 energy and water cycle components. This site has an about 8-10 cm deep organic forest-floor soil
399 horizon, typical of boreal deciduous broadleaf forests. When including, for the first time, an
400 organic-soil parameterization within the Noah-MP model, simulated sensible heat flux and latent
401 heat flux are improved in spring, especially in wet years, which is mostly related to the timing of
402 spring soil thaw and warming. However, in summer the model overestimated sensible heat fluxes.
403 Such high bias in summer sensible heat flux is largely attributed to surface-energy imbalance in
404 observations, especially in dry years. Due to lower thermal conductivity, the OGN simulated soil
405 temperature was decreased during summer and slightly increased during winter compared with
406 the CTL simulation, and the OGN simulated soil temperature (10-100cm) were more consistent
407 with observations and with previous studies (Lawrence and Slater 2008). Simulated top-layer
408 soil moisture is better in OGN than in CTL in summer but worse in winter.
409 Also, due to higher porosity of the organic soil, the OGN simulation was able to retain
410 more soil water content in summer. However, the effects of including an organic soil layer on

411 soil temperature are not uniform throughout the soil depth and year, and those effects are more
412 prominent in summer and in deep soils.

413 For drought years, the OGN simulation substantially modified the partition between
414 direct soil evaporation and vegetation transpiration. When water is limited in drought years, the
415 OGN simulation slightly increased the direct soil evaporation and produced higher summer total
416 evapotranspiration. Increased latent heat flux and sensible heat flux in summer in OGN are
417 compensated by decreased soil heat flux, leading to reduced soil temperature in summer. For wet
418 years, the OGN simulated latent heat fluxes are similar to CTL except for spring season where
419 OGN produced less evaporation. In addition, the impact of the organic soil on sub-surface runoff
420 is substantial with much higher runoff in freezing periods and lower runoff in summer season.

421 This preliminary study explored the effects of incorporating organic soil parameterization
422 in Noah-MP on the surface energy and water cycles for one flux site in a boreal forest area.
423 Given the important role of boreal forests in the regional climate system through reducing winter
424 albedo and also acting as a carbon sink and water source to the atmosphere, further work is
425 needed to evaluate the Noah-MP with organic-soil parameterization at regional scales. We plan
426 to evaluate the performance of the offline Noah-MP model and Noah-MP coupled with WRF for
427 a broad boreal forest region including Alberta and Saskatchewan.

428

429

430

431 **Acknowledgments**

432 The author Liang Chen acknowledge the support from the National Basic Research Program
433 (Grant No. 2012CB956203) and National Natural Science Foundation of China (Grant No.

41305062). The authors Liang Chen, Yanping Li, Alan Barr gratefully acknowledge the support from Global Institute of Water Security at University of Saskatchewan. Fei Chen, Michael Barlage and Bingcheng Wan appreciate the support from the Water System Program at the National Center for Atmospheric Research (NCAR), and NOAA MAPP-CTB grant (NA14OAR4310186). NCAR is sponsored by the National Science Foundation. Any opinions, findings, conclusions or recommendations expressed in this publication are those of the authors and do not necessarily reflect the views of the National Science Foundation.

References

Amiro BD, AG Barr, TA Black, H Iwashita, N Kljun, JH McCaughey, K Morgenstern, S Murayama, Z Nesic, AL Orchansky, and N Saigusa. 2006. Carbon, energy and water fluxes at mature and disturbed forest sites, Saskatchewan, Canada. Agric. For. Meteorol., 136: 237-251.

Ball, J. T., I. E. Woodrow, and J. A. Berry (1987), A model predicting stomatal conductance and its contribution to the control of photosynthesis under different environmental conditions, in Process in Photosynthesis Research, vol. 1, edited by J. Biggins, pp. 221–234, Martinus Nijhoff, Dordrecht, Netherlands.

Barlage, M., Tewari, M., Chen, F., Miguez-Macho, G., Yang, Z. L., and Niu, G. Y. (2015), The effect of groundwater interaction in North American regional climate simulations with WRF/Noah-MP, Climatic Change, 129(3-4), 485-498.

Bartlett, P.A., J.H. McCaughey, P.M. Lafleur and D.L. Verseghy (2002), A comparison of the mosaic and aggregated canopy frameworks for representing surface heterogeneity in the Canadian boreal forest using CLASS: A soil perspective, Journal of Hydrology, 266:15-39.

Barr, A. G., T. A. Black, E. H. Hogg, N. Kljun, K. Morgenstern, and Z. Nesic (2004), Inter-annual variability in the leaf area index of a boreal aspen-hazelnut forest in relation to net ecosystem production, Agricultural and forest meteorology, 126(3), 237–255.

Barr, A.G., K. Morgenstern, T. A. Black, J. H. McCaughey, and Z. Nesic (2006), Surface energy balance closure by the eddy-covariance method above three boreal forest stands and implications for the measurement of the CO2 flux, Agricultural and forest meteorology, 140, 322-337.

464 Beringer, J., N. J. Tapper, I. McHugh, F. Chapin, A. H. Lynch, M. C. Serreze, and A. Slater
465 (2001), Impact of arctic treeline on synoptic climate, Geophysical Research Letters, 28(22),
466 4247–4250.
467 Boelter, D. H. (1968), Important physical properties of peat materials. Proceedings of the 3rd
468 International Peat Congress, Quebec: 150-156.
469 Bonan, G. B. (1991), Atmosphere-biosphere exchange of carbon dioxide in boreal forests, J.
470 Geophys. Res., 96(D4), 7301–7312, doi: 10.1029/90JD02713.
471 Bonan, G. B., D. Pollard, and S. L. Thompson. 1992. Effects of Boreal Forest Vegetation on
472 Global Climate. Nature, 359: 716-18.
473 Bonan, G. B. (1997), Effects of land use on the climate of the United States, Climatic Change, 37,
474 449–486.
475 Brutsaert, W. A. (1982), Evaporation Into the Atmosphere, 299 pp., D. Reidel, Dordrecht,
476 Netherlands.
477 Bryant, D., D. Nielsen, and L. Tangley (1997), The Last Frontier Forests: Ecosystems and
478 Economies on the Edge. World Resources Institute.
479 Cai, X., Z. L. Yang, C. H. David, G. Y. Niu, and M. Rodell (2014), Hydrological evaluation of
480 the Noah‐MP land surface model for the Mississippi River Basin, Journal of Geophysical
481 Research: Atmospheres, 119(1), 23-38.
482 Chen, F., J. Dudhia (2001), Coupling an advanced land surface-hydrology model with the Penn
483 State-NCAR MM5 modeling system. Part I: Model implementation and sensitivity, Monthly
484 Weather Review, 129(4), 569-585.
485 Chen, F., K. Mitchell, J. Schaake, Y. Xue, H. L. Pan, V. Koren, Q. Y. Duan, M. Ek, and A. Betts
486 (1996), Modeling of land surface evaporation by four schemes and comparison with fife

observations, Journal of Geophysical Research: Atmospheres (1984–2012), 101(D3), 7251–7268.

Chen, F., M. J. Barlage, M. Tewari, R. M. Rasmussen, J. Jin, D. Lettenmaier, B. Livneh, C. Lin, G. Miguez-Macho, G. Y. Niu, L. Wen, and Z. L. Yang (2014), Modeling seasonal snowpack evolution in the complex terrain and forested Colorado Headwaters region: A model intercomparison study, Journal of Geophysical Research-Atmospheres, 119, 13795-13819, DOI: 10.1002/2014JD022167.

Chen, F. and K. Mitchell (1999), Using GEWEX/ISLSCP forcing data to simulate global soil moisture fields and hydrological cycle for 1987-1988, Journal of the Meteorological Society of Japan, 77, 1-16.

Chen F., G. Zhang, M. Barlage, Y. Zhang, J. A. Hicke, A. Meddens, G. Zhou, W. J. Massman, and J. Frank (2015), An Observational and Modeling Study of Impacts of Bark Beetle–Caused Tree Mortality on Surface Energy and Hydrological Cycles. J. Hydrometeor, 16, 744–761, doi: http://dx.doi.org/10.1175/JHM-D-14-0059.1

Chotamonsak, C., E. P. Salathe Jr, J. Kreasuwan, and S. Chantara (2012), Evaluation of precipitation simulations over Thailand using a WRF regional climate model. Chiang Mai Jounal of Science, 39(4), 623-638.

Ciais, P., P. P. Tans, M. Trolier, J. W. C. White, and R. J. Francey (1995), A large northern hemisphere terrestrial CO2 sink indicated by the 13C/12C ratio of atmospheric CO2, SCIENCE-NEW YORK THEN WASHINGTON, 1098-1098.

Clapp, R. B., and G. M. Hornberger (1978), Empirical equations for some soil hydraulic properties, Water resources research, 14(4), 601-604.

509 Clark, M. P., et al. (2015), A unified approach for process-based hydrologic modeling: 1.
510 Modeling concept, Water Resour. Res., 51, 2498–2514, doi:10.1002/2015WR017198
511 Cosgrove, B. A., D. Lohmann, K. E. Mitchell, P. R. Houser, E. F. Wood, J. C. Schaake, A.
512 Robock, C. Marshall, J. Sheffield, Q. Duan, L. Luo, R. W. Higgins, R. T. Pinker, J. D.
513 Tarpley, and J. Meng (2003), Real-time and retrospective forcing in the North American
514 Land Data Assimilation System (NLDAS) project, J. Geophys. Res., 108, 8842, doi:
515 10.1029/2002JD003118, D22.
516 Dai, Y., X. Zeng, R. E. Dickinson, I. Baker, G. B. Bonan, M. G. Bosilovich, A. S. Denning, P. A.
517 Dirmeyer, P. R. Houser, G. Niu, K. W. Oleson, C. A. Schlosser, and Z. L. Yang (2003), The
518 Common Land Model. Bull. Amer. Meteor. Soc., 84, 1013–1023. doi:
519 http://dx.doi.org/10.1175/BAMS-84-8-1013
520 Dickinson, R. E. (1986), Biosphere/atmosphere transfer scheme (bats) for the ncar com- munity
521 climate model, Technical report.
522 Dingman, S. L. (1994), Physical Hydrology, MacMillan Publishing Company, New York.
523 Ek, M. B., K. E. Mitchell, Y. Lin, E. Rogers, P. Grunmann, V. Koren, G. Gayno, and J. D.
524 Tarpley (2003), Implementation of Noah land surface model advances in the National
525 Centers for Environmental Prediction operational mesoscale Eta model, J. Geophys. Res.,
526 108, 8851, doi:10.1029/2002JD003296, D22.
527 Farouki, O. T. (1981), Thermal properties of soils, Report No. Vol. 81, No. 1, CRREL
528 Monograph
529 Gayler, S., T. Wöhling, M. Grzeschik, J. Ingwersen, H. D. Wizemann, K. Warrach-Sagi, P. Högy,
530 S. Attinger, T. Streck, and V. Wulfmeyer (2014), Incorporating dynamic root growth

531 enhances the performance of Noah-MP at two contrasting winter wheat field sites, Water
532 Resour. Res., 50, 1337-1356, doi:10.1002/ 2013WR014634.
533 Jordan, R. (1991), A one-dimensional temperature model for a snow cover, Spec. Rep. 91–16,
534 Cold Reg. Res. and Eng. Lab., U.S. Army Corps of Eng., Hanover, N. H.
535 Koren, V., J. C. Schaake, K. E. Mitchell, Q.-Y. Duan, F. Chen, and J. M. Baker (1999), A
536 parameterization of snowpack and frozen ground intended for NCEP weather and climate
537 models, J. Geophys. Res., 104, 19,569–19,585, doi:10.1029/1999JD900232.
538 Koven, C., P. Friedlingstein, P. Ciais, D. Khvorostyanov, G. Krinner, and C. Tarnocai (2009),
539 On the formation of high-latitude soil carbon stocks: Effects of cryoturbation and insulation
540 by organic matter in a land surface model, Geophys. Res. Lett., 36, L21501,
541 doi:10.1029/2009GL040150.
542 Lawrence, D. M., and A. G. Slater (2008), Incorporating organic soil into a global climate model,
543 Climate Dynamics, 30(2-3), 145–160.
544 Letts, M. G., N. T. Roulet, N. T. Comer, M. R. Skarupa, and D. L. Verseghy (2000),
545 Parametrization of peatland hydraulic properties for the Canadian land surface scheme,
546 Atmosphere-Ocean, 38(1), 141–160.
547 Levine, E. R., and R. G. Knox (1997), Modeling soil temperature and snow dynamics in northern
548 forests, J. Geophys. Res., 102(D24), 29407–29416, doi:10.1029/97JD01328.
549 Mölders, N., and V. E. Romanovsky (2006), Long-term evaluation of the Hydro-
550 Thermodynamic Soil-Vegetation Scheme's frozen ground/permafrost component using
551 observations at Barrow, Alaska, J. Geophys. Res., 111, D04105, doi:10.1029/2005JD005957.

552 Nicolsky, D. J., V. E. Romanovsky, V. A. Alexeev, and D. M. Lawrence (2007), Improved
553 modeling of permafrost dynamics in a GCM land-surface scheme, Geophys. Res. Lett., 34,
554 L08501, doi:10.1029/2007GL029525.
555 Niu, G.-Y., and Z.-L. Yang (2006), Effects of frozen soil on snowmelt runoff and soil water
556 storage at a continental scale, J. Hydrometeorol., 7, 937–952, doi:10.1175/JHM538.1.
557 Niu, G.-Y., Z.-L. Yang, R. E. Dickinson, and L. E. Gulden (2005), A simple TOPMODEL-based
558 runoff parameterization (SIMTOP) for use in global climate models, J. Geophys. Res., 110,
559 D21106, doi:10.1029/2005JD006111.
560 Niu, G. Y., Z. L. Yang, K. E. Mitchell, F. Chen, M. B. Ek, M. Barlage, A. Kumar, K. Manning,
561 D. Niyogi, and E. Rosero (2011), The community Noah land surface model with
562 multiparameterization options (Noah-MP): 1. Model description and evaluation with local-
563 scale measurements, J. Geophys. Res., 116, D12109, doi:10.1029/2010JD015139.
564 Oleson, K. W., G. Y. Niu, Z. L. Yang, D. M. Lawrence, P. E. Thornton, P. J. Lawrence, R.
565 Stöckli, R. E. Dickinson, G. B. Bonan, S. Levis, A. Dai, and T. Qian (2008), Improvements
566 to the Community Land Model and their impact on the hydrological cycle, J. Geophys. Res.,
567 113, G01021, doi: 10.1029/2007JG000563.
568 Pilotto, I. L., Rodríguez, D. A., Tomasella, J., Sampaio, G., and Chou, S. C. (2015),
569 Comparisons of the Noah-MP land surface model simulations with measurements of forest
570 and crop sites in Amazonia. Meteorology and Atmospheric Physics, 127(6), 711-723, doi:
571 10.1007/s00703-015-0399-8.
572 Radforth, N. W. and Brawner, C. O. (1977). Muskeg and the northern environment in Canada. In
573 Muskeg Research Conference 1973: Edmonton, Alberta. University of Toronto Press.

574 Rinke, A., P. Kuhry, and K. Dethloff (2008), Importance of a soil organic layer for Arctic
575 climate: A sensitivity study with an Arctic RCM, Geophys. Res. Lett., 35, L13709,
576 doi:10.1029/2008GL034052.
577 Thomas, G. and Rowntree, P. R. (1992), The Boreal Forests and Climate. Q.J.R. Meteorol. Soc.,
578 118, 469–497. doi: 10.1002/qj.49711850505
579 Verseghy, D. L. (1991), CLASS-A Canadian land surface scheme for GCMS: I. Soil model, Int.
580 J. Climatol., 11, 111–133, doi:10.1002/joc.3370110202.
581 Viterbo, P., and A. K. Betts (1999), Impact on ECMWF forecasts of changes to the albedo of the
582 boreal forests in the presence of snow, J. Geophys. Res., 104(D22), 27803–27810,
583 doi:10.1029/1998JD200076.
584 Yang, Z. L., R. E. Dickinson, A. Henderson-Sellers, and A. J. Pitman (1995), Preliminary study
585 of spin-up processes in land surface models with the first stage data of project for
586 intercomparison of land surface parameterization schemes phase 1 (a), Journal of
587 Geophysical Research: Atmospheres, 100 (D8), 16,553–16,578.
588 Yang, Z.-L., G.-Y. Niu, K. E. Mitchell, F. Chen, M. B. Ek, M. Barlage, L. Longuevergne, K.
589 Manning, D. Niyogi, M. Tewari, and Y. Xia (2011), The community Noah land surface
590 model with multiparameterization options (Noah-MP): 2. Evaluation over global river basins,
591 J. Geophys. Res., 116, D12110, doi:10.1029/2010JD015140.
592 Zhang, G., G. Zhou, F. Chen, M. Barlage, and L. Xue (2014), A trial to improve surface heat
593 exchange simulation through sensitivity experiments over a desert steppe site, J.
594 Hydrometeor, 15(2), 664–684, doi:10.1175/jhm-d-13-0113.1.
595 Zheng, D., et al. (2015), Under-canopy turbulence and root water uptake of a Tibetan meadow
596 ecosystem modeled by Noah-MP, Water Resour. Res., 51, doi:10.1002/2015WR017115
597

598
599 Table 1. Noah-MP Parameterization Options Used in this Study

Patameterizations Description	Options
Dynamic vegetation	4: table LAI, shdfac=maximum
Stomatal resistance	1: BALL-Berry (Ball et al., 1987)
Soil moisture factor for stomatal resistance	1: original Noah (Chen and Dudhia, 2001)
Runoff/soil lower boundary	2: TOPMODEL with equilibrium water table (Niu et al. 2005)
Surface layer drag Coefficient calculation	1: Monin-Obukhov (Brutsaert, 1982)
Supercooled liquid water	1: no iteration (Niu and Yang, 2006)
Soil permeability	1: linear effects, more permeable (Niu and Yang, 2006)
Radiative transfer	3: two-stream applied to vegetated fraction
Ground surface albedo	2: CLASS (Verseghy, 1991)
Precipitation partitioning between snow and rain	1: Jordan (Jordan, 1991)
soil temp lower boundary	2: TBOT at ZBOT (8m) read from a file
snow/soil temperature time	1: semi-implicit

600

601 Table 2 Soil parameters used in Noah-MP for mineral soil texture classes (SANDY CLAY

602 LOAM) and organic soil (Hemic Peat).

Soil Type	λ_s (w m^{-1} K^{-1})	λ_{sat} (w m^{-1} K^{-1})	λ_{dry} (w m^{-1} K^{-1})	c_s (J m^{-3} $K^{-1}\cdot10^6$)	θ_{sat}	κ_{sat} (m $s^{-1}\times10^{-3}$)	ψ_{sat} (mm)	b
Mineral	6.04	2.24	0.23	2.0	0.421	0.00445	-135	6.77
Organic	0.25	0.55	0.05	2.5	0.88	0.002	-10.3	6.1

603 The soil parameters are λ_s is the thermal conductivity of soil solids, λ_{sat} is the unfrozen saturated
604 thermal conductivity, λ_{dry} is the dry soil thermal conductivity, c_s is the soil solid heat capacity,
605 θ_{sat} is the saturated volumetric water content (porosity), κ_{sat} is the saturate hydraulic conductivity,
606 ψ_{sat} is the saturated matric potential, and b is the Clapp and Hornberger parameter.

607 **Table 3.** Averaged statistical indices for CTL and OGN simulated SH and LH compared with
608 the observations for each year [daytime, 0800-1600 local time (LT)] (R^2: correlation coefficient
609 square; RMSE: root mean square error; IOA: index of agreement).

Year	SH						LH					
	CTL			OGN			CTL			OGN		
	R^2	RMSE	IOA	R^2	RMSE	IOA	R^2	RMSE	IOA	R^2	RMSE	IOA
1998	0.56	80.92	0.83	0.65	81.40	0.85	0.72	51.00	0.91	0.76	47.70	0.93
1999	0.64	64.30	0.88	0.69	68.59	0.88	0.74	44.52	0.92	0.76	43.01	0.93
2000	0.62	71.20	0.87	0.68	74.27	0.88	0.70	47.46	0.90	0.71	46.19	0.91
2001	0.72	63.09	0.90	0.78	66.84	0.91	0.78	40.36	0.93	0.81	36.85	0.95
2002	0.75	69.60	0.91	0.77	71.41	0.92	0.69	37.24	0.91	0.70	39.66	0.91
2003	0.77	56.52	0.93	0.79	56.74	0.94	0.72	36.45	0.91	0.73	42.02	0.90
2004	0.72	61.88	0.91	0.75	64.82	0.92	0.73	39.84	0.92	0.74	40.15	0.92
2005	0.69	60.98	0.90	0.76	60.59	0.92	0.73	43.29	0.92	0.78	39.75	0.94
2006	0.60	67.70	0.86	0.68	70.16	0.88	0.77	49.58	0.93	0.80	45.36	0.94
2007	0.65	65.15	0.89	0.72	65.28	0.90	0.76	46.79	0.93	0.81	42.49	0.95
2008	0.71	63.54	0.91	0.76	68.15	0.91	0.76	44.95	0.93	0.80	40.79	0.95
2009	0.69	66.52	0.90	0.72	69.38	0.90	0.72	43.77	0.91	0.74	43.32	0.92

610

Figure Captions:

Figure 1. The location of the study site (Old Aspen Flux Tower)

Figure 2. Monthly air temperature above canopy and precipitation at BERMS SK-OAS site

Figure 3. Averaged spin-up time (in years) for individual variables.

Figure 4. Observed and Noah-MP-simulated monthly soil temperature for BERMS SK-OAS site at a depth of (a) top 10 cm, (b) 10-40 cm, and (c) 40-100 cm

Figure 5. Observed and Noah-MP-simulated monthly soil moisture for BERMS SK-OAS site at a depth of (a) top 10 cm, (b) 10-40 cm, and (c) 40-100 cm

Figure 6. Observed and the Noah-MP simulated (CTL and OGN) daytime monthly-average sensible and latent heat flux above canopy. *Error bars represent the average and deviations [(RN-G)×B/(1+B) for SH, and (RN-G)/(1+B) for LH] from observations, and B is the Bowen ratio (B=SH/LH)*.

Figure 7. Scatterplots of the daytime monthly-averaged (a) sensible, (b) latent heat fluxes (W m−2) for CTL versus the observation above canopy; the monthly-averaged (c) sensible, (d) latent heat fluxes (W m^{-2}) for OGN versus the observation above canopy. The color represents each month from January (1) to December (12).

Figure 8. Comparison of the seasonal averaged diurnal cycle of the sensible and latent heat fluxes at OAS site for drought years

Figure 9. Comparison of the seasonal averaged diurnal cycle of the sensible and latent heat fluxes at OAS site for wet years

Figure 10. Annual cycle of selected surface energy and hydrologic cycle fields for drought years. Black line is the observation. Note that (a) is the observed precipitation, (b) is sensible heat flux, (c) is latent heat flux, (d) is ground heat flux, (e) is surface runoff, (f) is underground runoff, (g)

634 is volumetric liquid water content for soil layer one, (h) is volumetric ice water content for soil
635 layer one.
636 **Figure 11.** Annual cycle of selected surface energy and hydrologic cycle fields for wet years.
637 Black line is the observation. Note that (a) is the observed precipitation, (b) is sensible heat flux,
638 (c) is latent heat flux, (d) is ground heat flux, (e) is surface runoff, (f) is underground runoff, (g)
639 is volumetric liquid water content for soil layer one, (h) is volumetric ice water content for soil
640 layer one.
641 **Figure 12.** Water budgets: blue lines are accumulated surface runoff (mm), blue dots are
642 accumulated underground runoff (mm), red lines are accumulated evaporation of intercepted
643 water (mm), red dots are accumulated ground surface evaporation (mm), red dash lines are
644 accumulated transpiration (mm), green lines are snow water equivalent changes (mm), purple
645 lines are soil water content changes in the soil column (mm), (a) and (b) are averaged for 2002–
646 2003, (c) and (d) are averaged for 2005-2006.
647

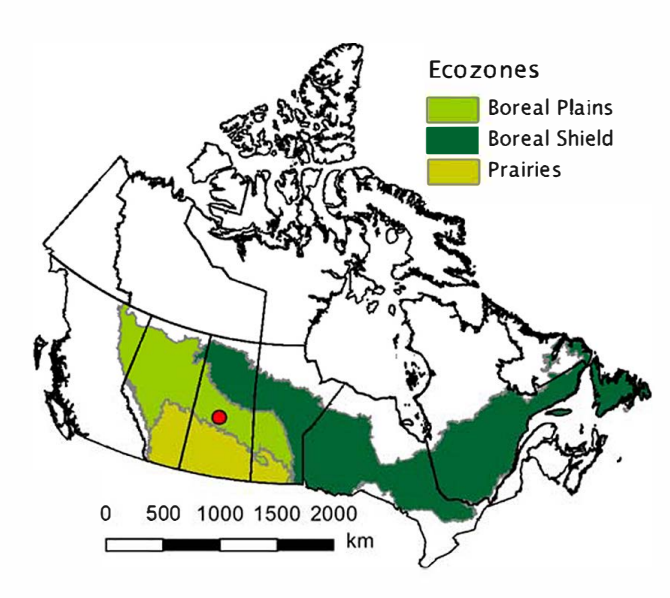

Figure 1. The location of the study site (Old Aspen Flux Tower)

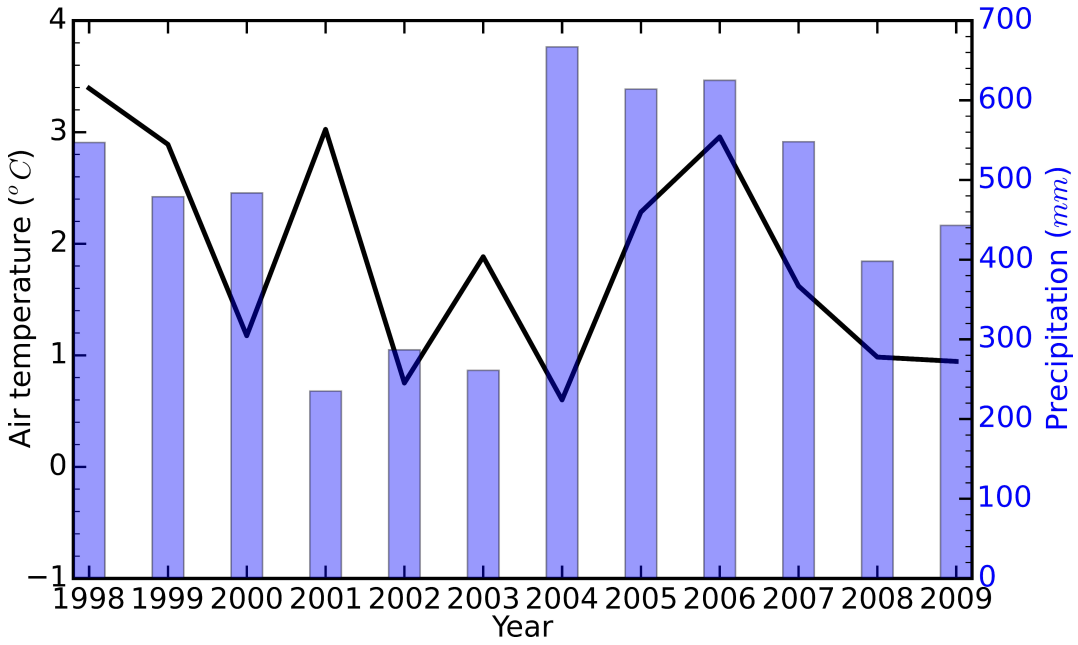

651

652 **Figure 2.** Monthly air temperature above canopy and precipitation at BERMS SK-OAS site

653

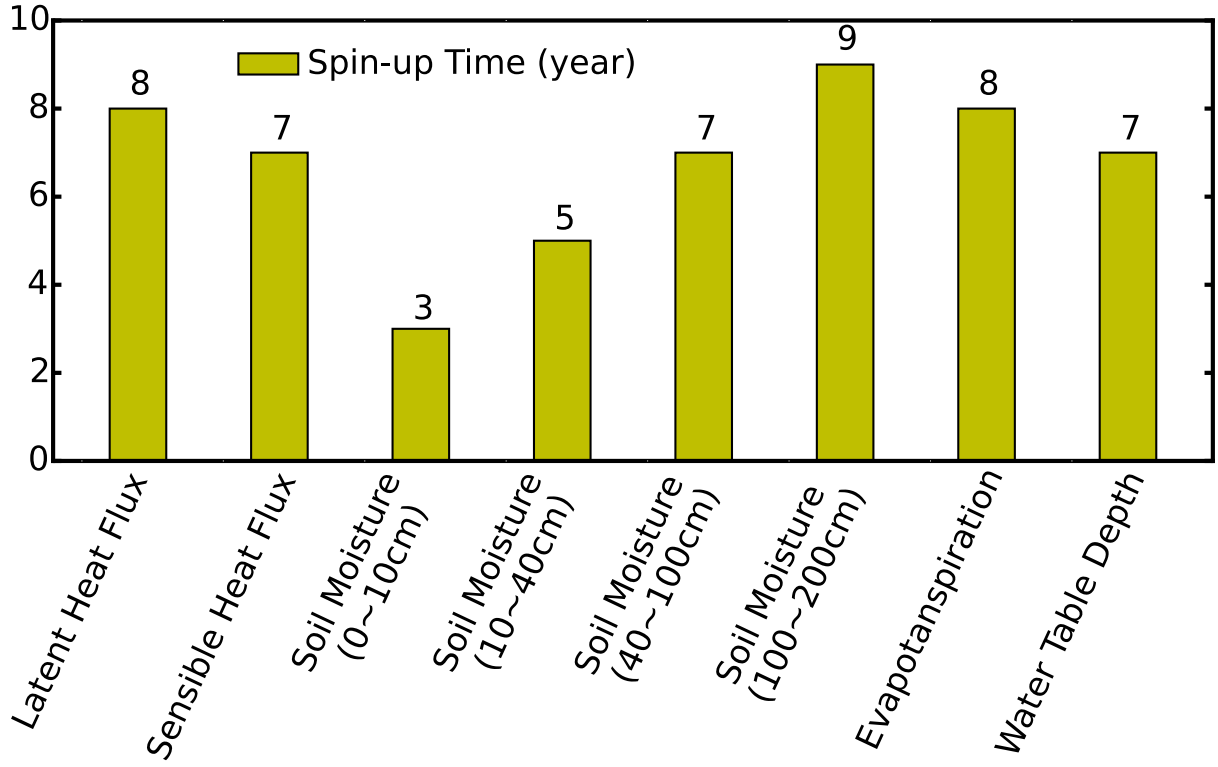

654

655 **Figure 3.** Averaged spin-up time (in years) for individual variables.

656

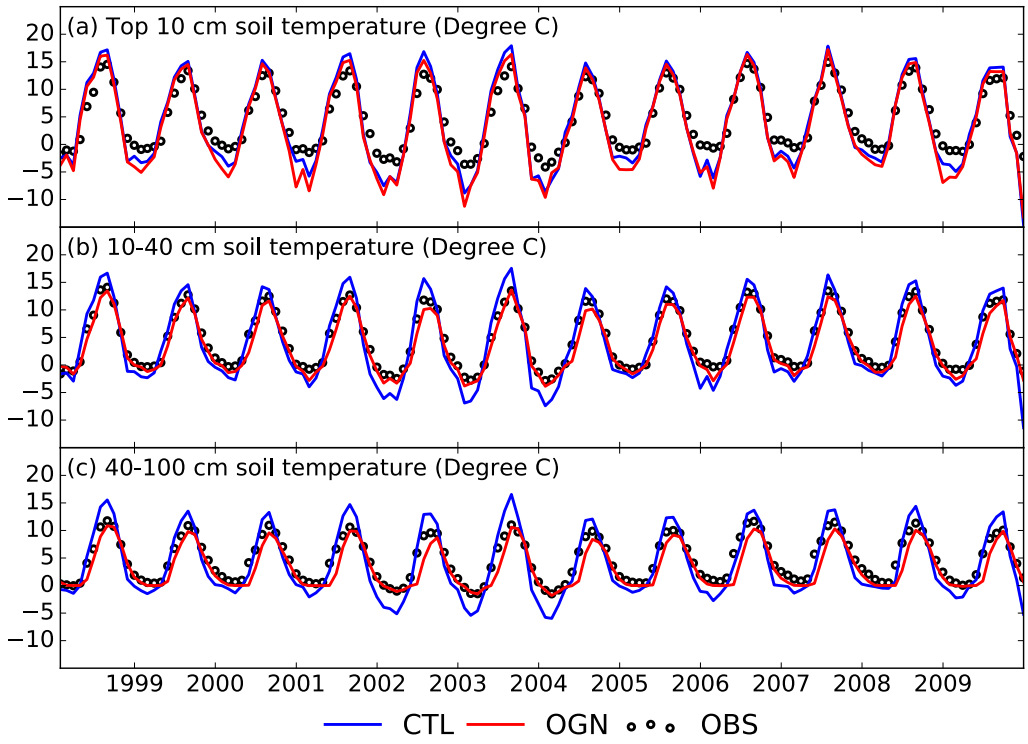

657

658 **Figure 4.** Observed and Noah-MP-simulated monthly soil temperature for BERMS SK-OAS site

659 at a depth of (a) top 10 cm, (b) 10-40 cm, and (c) 40-100 cm

660

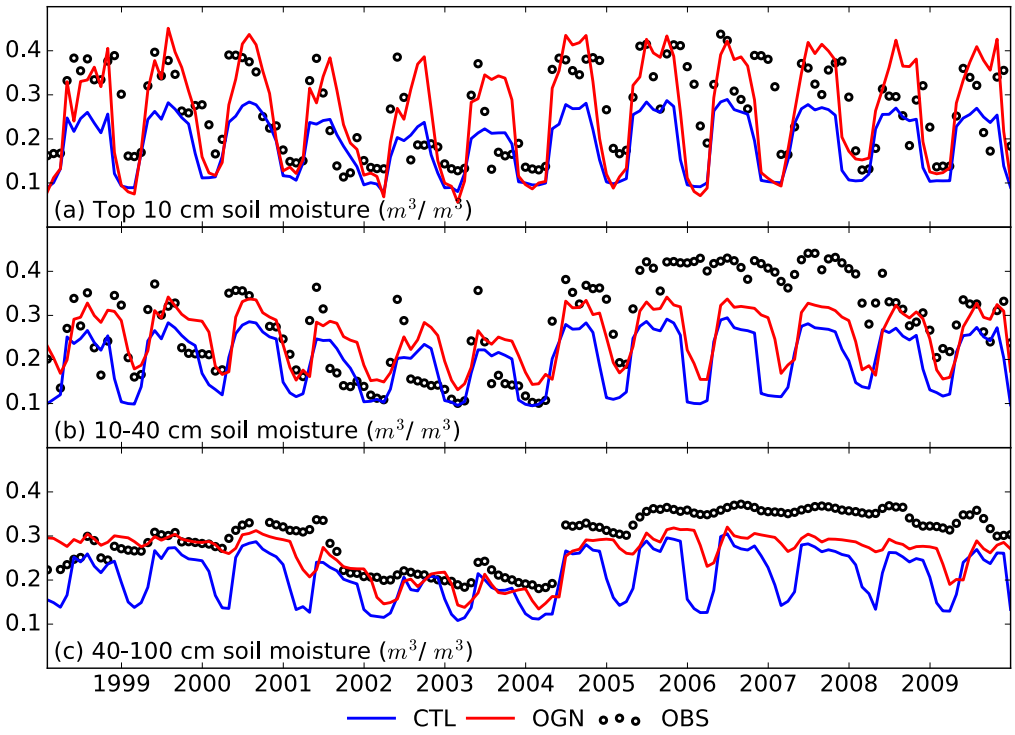

661

662 **Figure 5.** Observed and Noah-MP-simulated monthly soil moisture for BERMS SK-OAS site at

663 a depth of (a) top 10 cm, (b) 10-40 cm, and (c) 40-100 cm

664

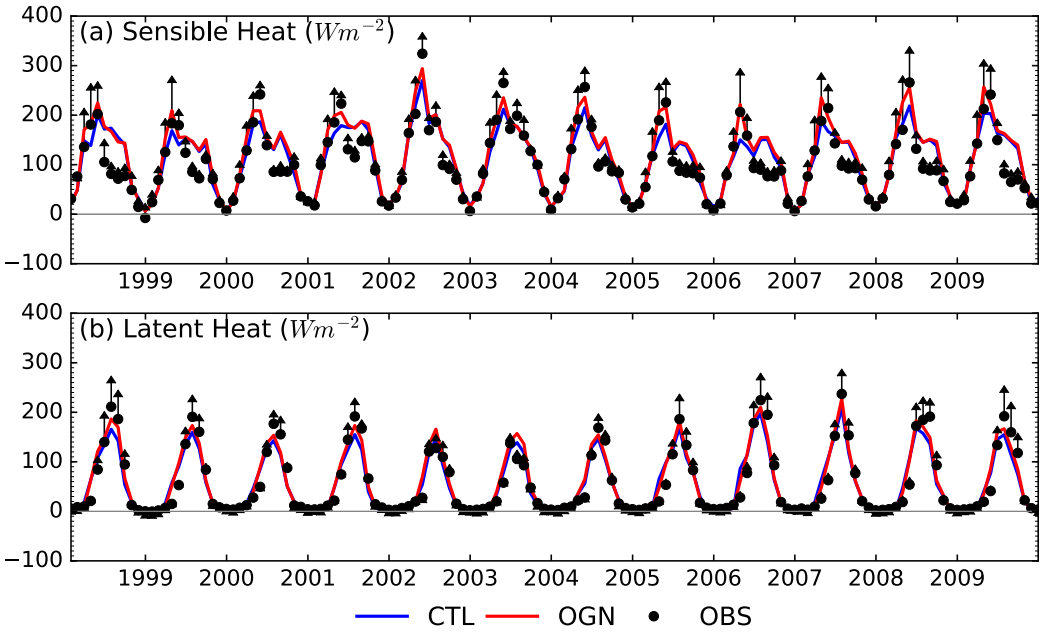

Figure 6. Observed and the Noah-MP simulated (CTL and OGN) daytime monthly-average sensible and latent heat flux above tree canopy. *Error bars represent the average and deviations [(RN-G)×B/(1+B) for SH, and (RN-G)/(1+B) for LH] from observations, and B is the Bowen ratio (B=SH/LH)*.

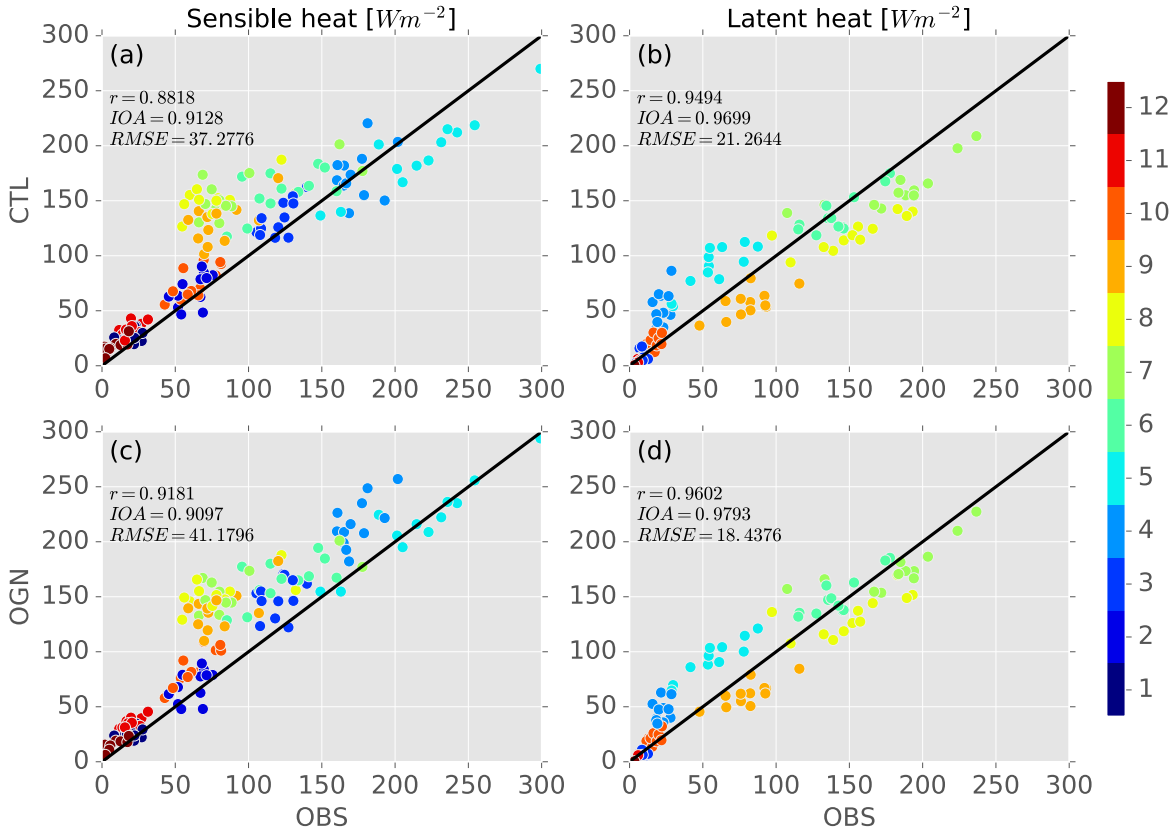

671

672 **Figure 7.** Scatterplots of the daytime monthly-averaged (a) sensible, (b) latent heat fluxes
673 (W m−2) for CTL versus the observation above canopy; the monthly-averaged (c) sensible, (d)
674 latent heat fluxes (W m^{-2}) for OGN versus the observation above canopy. The color represents
675 each month from January (1) to December (12).

676

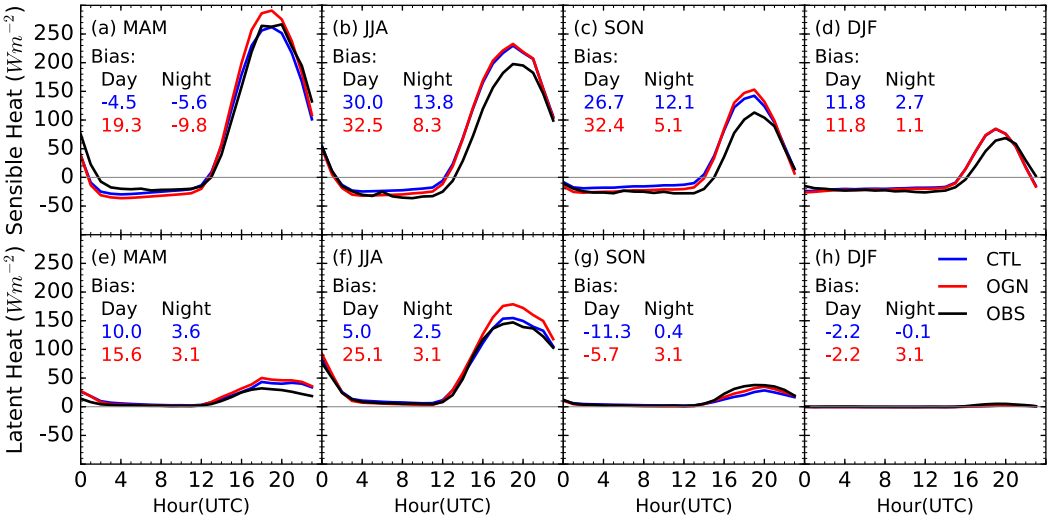

677

678 **Figure 8.** Comparison of the seasonal averaged diurnal cycle of the sensible and latent heat

679 fluxes at OAS site for drought years

680

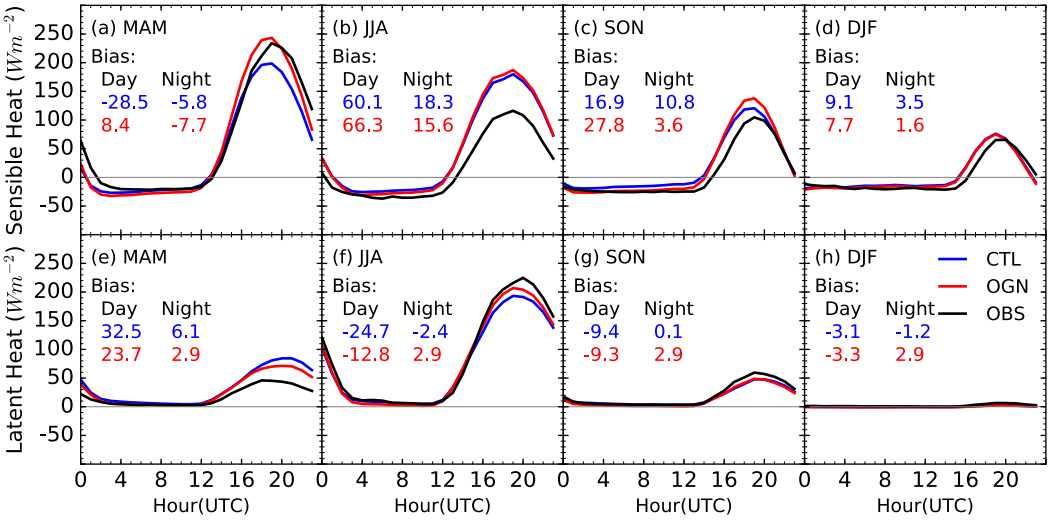

681

682 **Figure 9.** Comparison of the seasonal averaged diurnal cycle of the sensible and latent heat

683 fluxes at OAS site for wet years

684

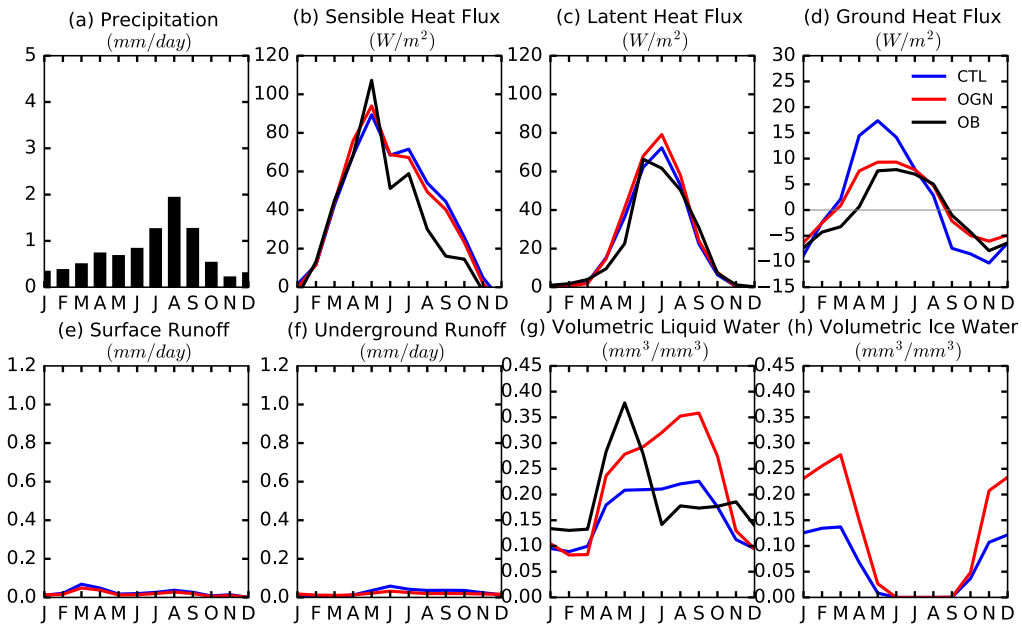

685

686 **Figure 10.** Annual cycle of selected surface energy and hydrologic cycle fields for drought years.

687 Black line is the observation. Note that (a) is the observed precipitation, (b) is sensible heat flux,

688 (c) is latent heat flux, (d) is ground heat flux, (e) is surface runoff, (f) is underground runoff, (g)

689 is volumetric liquid water for soil layer one, (h) is volumetric ice water content for soil layer one.

690

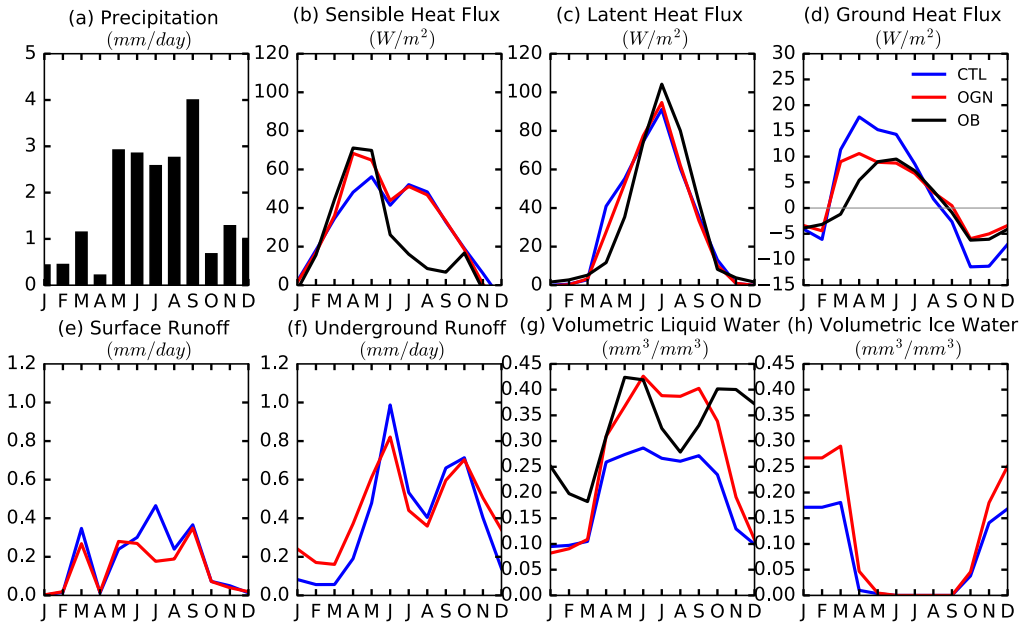

691

692 **Figure 11.** Annual cycle of selected surface energy and hydrologic cycle fields for wet years.
693 Black line is the observation. Note that (a) is the observed precipitation, (b) is sensible heat flux,
694 (c) is latent heat flux, (d) is ground heat flux, (e) is surface runoff, (f) is underground runoff, (g)
695 is volumetric liquid water content for soil layer one, (h) is volumetric ice water content for soil
696 layer one.

697

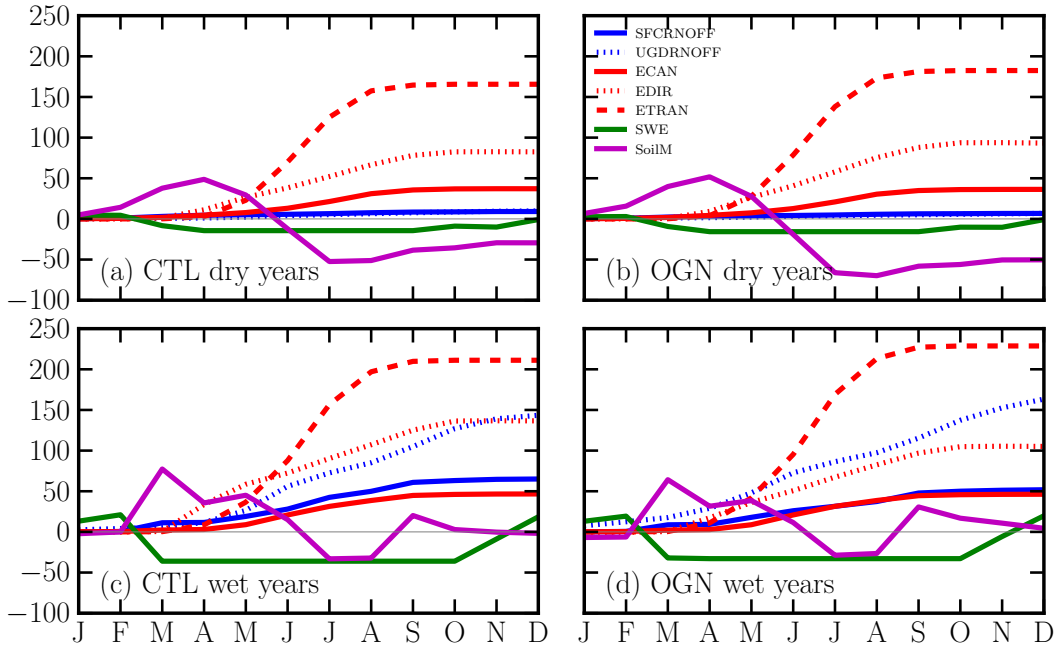

698

699 **Figure 12.** Water budgets: blue lines are accumulated surface runoff (mm), blue dots are
700 accumulated underground runoff (mm), red lines are accumulated evaporation of intercepted
701 water (mm), red dots are accumulated ground surface evaporation (mm), red dash lines are
702 accumulated transpiration (mm), green lines are snow water equivalent changes (mm), purple
703 lines are soil water content changes in the soil column (mm), (a) and (b) are averaged for 2002–
704 2003, (c) and (d) are averaged for 2005-2006.